β-Catenin–dependent mechanotransduction dates back to the common ancestor of Cnidaria and Bilateria

Ekaterina Pukhlyakova[a], Andrew J. Aman[a,1], Kareem Elsayad[b], and Ulrich Technau[a,2]

[a]Department for Molecular Evolution and Development, Centre of Organismal Systems Biology, University of Vienna, Vienna A-1090, Austria; and [b]Advanced Microscopy Section, Vienna Biocenter Core Facilities GmbH, Vienna A-1030, Austria

Edited by Richard M. Harland, University of California, Berkeley, CA, and approved April 30, 2018 (received for review August 3, 2017)

Although the genetic regulation of cellular differentiation processes is well established, recent studies have revealed the role of mechanotransduction on a variety of biological processes, including regulation of gene expression. However, it remains unclear how universal and widespread mechanotransduction is in embryonic development of animals. Here, we investigate mechanosensitive gene expression during gastrulation of the starlet sea anemone *Nematostella vectensis*, a cnidarian model organism. We show that the blastoporal marker gene *brachyury* is downregulated by blocking myosin II-dependent gastrulation movements. *Brachyury* expression can be restored by applying external mechanical force. Using CRISPR/Cas9 and morpholino antisense technology, we also show that mechanotransduction leading to *brachyury* expression is β-catenin dependent, similar to recent findings in fish and *Drosophila* [Brunet T, et al. (2013) *Nat Commun* 4:1–15]. Finally, we demonstrate that prolonged application of mechanical stress on the embryo leads to ectopic *brachyury* expression. Thus, our data indicate that β-catenin–dependent mechanotransduction is an ancient gene regulatory mechanism, which was present in the common ancestor of cnidarians and bilaterians, at least 600 million years ago.

Nematostella | mechanotransduction | β-catenin | gastrulation | *brachyury*

Embryonic development is governed by a genetic program, which includes numerous feedback loops and ramifications. However, the role of epigenetic cues and physical constraints in influencing development has recently gained support. Mechanical forces can be transformed by cells into biochemical signals in a process called mechanotransduction (1–9). Parameters like cell shape, ability to spread on extracellular matrix, and stiffness of the cell environment can directly govern cell differentiation and proliferation rate (10–15). Recent experimental studies have begun to elucidate roles for mechanotransduction in embryonic development, such as regulation of gene expression, pattern fomation, and organogenesis (16–22). In *Drosophila*, external mechanical stress induced the key mesoderm determinant *twist*, while in zebrafish, mechanical stress induced expression of *brachyury*, which is crucial for mesoderm development in all vertebrates. Notably, in both organisms, this mechanically induced gene expression is dependent on β-catenin (16). However, to date, it is unclear whether these are isolated phenomena or whether this reflects a conserved mechanism. To test whether mechanosensitive gene regulation predates the origin of Bilateria, we chose to study the anthozoan sea anemone *Nematostella vectensis*, a representative of the Cnidaria, the sister group to Bilateria, which emerged ∼600–700 Mya (23, 24). Interestingly, the *Nematostella* homolog of *brachyury* is expressed around the blastopore, and this expression pattern is conserved in most studied embryos, representing diverse bilaterian and nonbilaterian phyla (25–35). As in vertebrates and other deuterostomes, *brachyury* is a direct target of Wnt/β-catenin signaling (36–39). Thus, a blastoporal expression of *brachyury* and its regulation seems to be a widely conserved feature among metazoans (25–35).

Results

The Role of Myosin II During Gastrulation of *N. vectensis*. Gastrulation in *N. vectensis* occurs by invagination and is initiated by the apical constriction of cells at the animal pole, which leads to the formation of the preendodermal plate. Subsequently, the preendodermal plate invaginates into the blastocoel (Movie S1) (40, 41). As actomyosin constriction is involved in apical constriction and cell-shape changes, we examined the necessity of this force-generating mechanism during gastrulation using ML-7, a potent and selective reversible myosin light chain kinase (MLCK) inhibitor. We found that 10 μM ML-7, applied at blastula stage, was sufficient to completely inhibit invagination during gastrulation, although this treatment did not entirely inhibit apical constriction of preendodermal cells (Fig. 1*I*) (42, 43). It is likely that additional, actomyosin-independent mechanisms such as membrane shuttling participate in preendoderm apical constriction (44). To show that the effect of ML-7 is nontoxic and reversible, we washed out the inhibitor after 12 h of treatment, at the time when the control embryos have completed gastrulation. Most of the ML-7 washout embryos (78/100) then gastrulated (Fig. S1) and ultimately develop into polyps. Thus, ML-7 specifically impairs myosin II function required for invagination of the endoderm during *N. vectensis* gastrulation.

Significance

Besides genetic regulation, mechanical forces have been identified as important cues in numerous developmental processes. Mechanical forces can activate biochemical cascades in a process called mechanotransduction. Recent studies in vertebrates and flies elucidated the role of mechanical forces for mesodermal gene expression. However, it remains unclear whether mechanotransduction is a universal regulatory mechanism throughout Metazoa. Here, we show in the sea anemone *Nematostella vectensis* that mechanical pressure can ectopically activate or restore *brachyury* expression. This mechanotransduction is dependent on β-catenin, similar to vertebrates. We propose that a regulatory feedback loop between genetic and mechanical gene activation exists during gastrulation and the β-catenin–dependent mechanotransduction is an ancient regulatory mechanism, which was present in the common ancestor of cnidarians and bilaterians.

Author contributions: E.P., A.J.A., and U.T. designed research; E.P. and A.J.A. performed research; K.E. contributed new reagents/analytic tools; E.P., A.J.A., K.E., and U.T. analyzed data; and E.P., A.J.A., and U.T. wrote the paper.

The authors declare no conflict of interest.

This article is a PNAS Direct Submission.

[1]Present address: Department of Biology, University of Virginia, Charlottesville, VA 22904.

[2]To whom correspondence should be addressed. Email: ulrich.technau@univie.ac.at.

This article contains supporting information online at www.pnas.org/lookup/suppl/doi:10.1073/pnas.1713682115/-/DCSupplemental.

Published online May 21, 2018.

DEVELOPMENTAL BIOLOGY

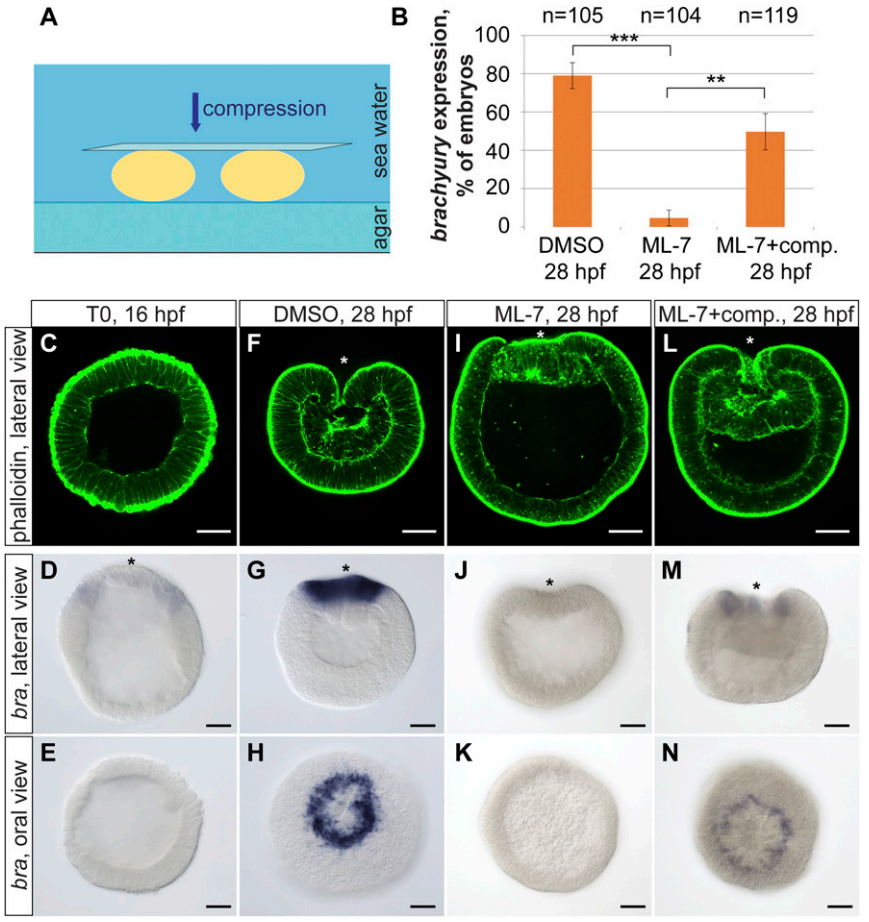

Fig. 1. Mechanically induced *brachyury* expression in the *Nematostella* embryos. (*A*) Scheme of the compression experiment. Embryos are compressed by a coverslip in seawater. (*B*) Quantification of the embryos, expressing *brachyury* upon DMSO control, treatment with ML-7 alone, and treatment with ML-7 combined with mechanical compression. Data from at least three independent experiments are combined and displayed in the graph. Differences between DMSO and ML-7–treated embryos, and between ML-7–treated and ML-7–treated/compressed embryos, are significant, paired two-tailed Student's *t* test (***$P < 0.01$; **$P < 0.02$). (*C–E*) Earliest detectable onset of the ring-like *brachyury* expression in blastulae at 16 hpf marking the presumptive blastopore lip. (*F–H*) *Brachyury* expression in the DMSO-treated control embryos at late gastrula stage (28 hpf). (*I–K*) Gastrulae treated from 16 to 28 hpf with ML-7 show inhibition of invagination of preendodermal plate as well as loss or severe down-regulation of *brachyury* expression. (*L–N*) Mechanical uniaxial global compression can rescue *brachyury* expression in the ML-7–treated embryos. (Scale bar, 50 μm.) Asterisk indicates the oral pole of the embryo.

Blocking Gastrulation Movements Inhibits *Brachyury* Expression, Which Can Be Rescued by Applying External Mechanical Stress. Gastrulation in *Nematostella* is accompanied by the expression of several marker genes. Expression of the T-box gene *brachyury* starts shortly before gastrulation as a broad ring at blastula stage marking the boundary of the preendodermal plate (Fig. 1 *C–E*) (45–48). With the beginning of gastrulation movements, *brachyury* expression intensifies and narrows to a few rows of marginal cells surrounding the blastopore (Fig. 1 *F–H*).

If *brachyury* expression depends on mechanical stress generated by gastrulation movements, we expected *brachyury* expression to be reduced in ML-7–treated embryos. Indeed, in more than 95% of ML-7–treated embryos *brachyury* expression either vanishes completely or is not expressed as a contiguous ring (Fig. 1 *B*, *J*, and *K*). To determine whether loss of *brachyury* expression in ML-7–inhibited embryos is due to the absence of mechanical strains, pregastrulation blastulae were subjected to external pressure for 12 h during ML-7 treatment (Fig. 1*A* and Fig. S2). As controls, spherical blastulae were treated with ML-7 or DMSO without exogenous force. Experimental treatments began in stage-matched blastulae [16 hours postfertilization (hpf)] and were terminated when all of the DMSO-treated control embryos had completed gastrulation (28 hpf). We observed normal *brachyury* expression in a contiguous ring in 50% ($n = 119$) of the ML-7–treated embryos subjected to compression compared with 5% ($n = 104$) in similarly treated embryos with no compression (three independent experiments; $P \leq 0.02$ paired, two-tailed Student's *t* test) (Fig. 1 *B*, *M*, and *N*). These data show that applied mechanical stimulation is sufficient to restore *brachyury* expression in embryos lacking gastrulation strains.

Interestingly, mechanical force applied to the ML-7–treated embryos during gastrulation activated *brachyury* expression only around the blastopore (Fig. 1*N*). Thus, blastoporal cells appear more competent than the rest of the embryo to respond to mechanical forces by altering gene expression, likely because the blastopore cells are a zone of active Wnt/β-catenin signaling and *brachyury* is a direct target of β-catenin (47, 48).

Up-Regulation of *Brachyury* Expression upon External Mechanical Strain Is β-Catenin Dependent. To test whether β-catenin has a role in stress-induced expression of *brachyury*, we used CRISPR/Cas9 technology to mutate the *apc* homolog in *Nematostella* (48–51). Apc is a necessary component of the β-catenin destruction complex and its loss of function is expected to lead to constitutive activation of Wnt/β-catenin signaling (52). Homozygous mutants of *apc* show a discernible phenotype at 3 dpf, as

expected for a negative regulator of Wnt signaling (47, 53). Homozygous *apc* mutants also express *brachyury* ectopically compared with wild-type and heterozygous siblings (Fig. 2 *A–D*). Importantly, this expression was maintained even during ML-7 treatment, which blocks invagination of the preendodermal plate (Fig. 2 *E* and *F*), suggesting that the stabilization of β-catenin is downstream of the mechanotransduction.

As a complementary test, we repeated the ML-7 treatment and application of mechanical strain on embryos where β-catenin expression is knocked down by morpholino (MO) injection (53). *Brachyury* expression was lost in the β-catenin morpholino-injected embryos and could not be rescued by application of external mechanical stress (Fig. 2 *G–K*). Together, these results show that up-regulation of *brachyury* expression upon mechanical stress is β-catenin dependent and that the mechanical stress acts upstream of β-catenin activation.

Prolonged Mechanical Stress Activates Ectopic *Brachyury* Expression. To test whether other areas of the embryo are competent to express *brachyury* in response to mechanical force, we subjected stage-matched spherical blastulae to prolonged compression. We compressed embryos at 15 °C for 26 h until control embryos had completed gastrulation. Incubation at colder temperatures slows down the development and enables the force impact during gastrulation for a longer time. About 40% (74/187) of the compressed embryos had broad, ectopic *brachyury* expression relative to ∼10% (7/68) uncompressed controls (Fig. 3 *A–C*). Interestingly, compression of late gastrulae did not lead to ectopic *brachyury* expression (Fig. 3 *D–F*). Hence, there appears to be a narrow time window in which cells are competent to respond to mechanical forces. This implies that mechanical forces cooperate with the genetic factors to regulate *brachyury* expression during the blastula-to-gastrula transition.

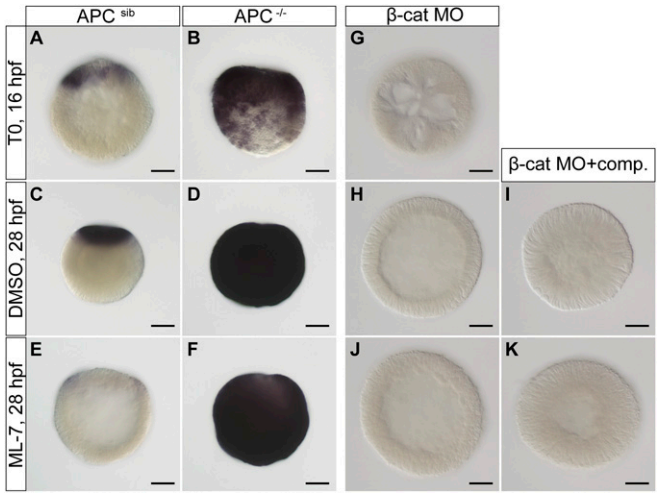

Fig. 2. Up-regulation of *brachyury* expression upon external mechanical strain is β-catenin dependent. (*A–D*) *Brachyury* is ectopically expressed in APC$^{-/-}$ homozygous mutants throughout embryonic development. (*E*) ML-7 leads to down-regulation of *brachyury* in wild-type or heterozygous embryos. (*F*) ML-7 treatment does not inhibit up-regulation of *brachyury* expression in APC$^{-/-}$ homozygous mutants. (*G* and *H*) β-Catenin morpholino injection leads to the complete inhibition of *brachyury* expression throughout the embryo development in control embryos. (*I* and *K*) Mechanical compression of β-catenin MO-injected embryos combined with DMSO control or ML-7 treatment does not rescue *brachyury* expression. (Scale bar, 50 μm.) APC$^{-/-}$, homozygous mutants; APC^{sib}, siblings, heterozygous mutants, or wild-type embryos.

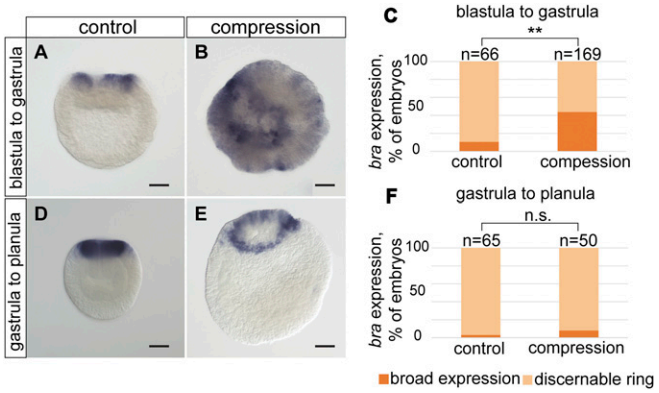

Fig. 3. Prolonged external mechanical stress can cause an overexpression or ectopic *brachyury* expression at blastula and early gastrula stage. (*A*) Control embryo expressing *brachyury* as a ring around the blastopore. (*B*) Overexpression of *brachyury* after long-term embryo compression, applied at blastula stage for 26 h. (*C*) Quantification of the embryos expressing *brachyury* at blastopore or ectopically. (**χ^2 test; $P < 0.01$) (*D*) Strong blastopore expression of *brachyury* in late control gastrula. (*E*) Late gastrula compressed for 26 h. No ectopic *brachyury* expression was detected. (*F*) Quantification of *brachyury* expression after late gastrula compression. Data are pooled from two independent experiments. The difference between control and compressed gastrulae is significant (n.s., nonsignificant; χ^2 test; **$P > 0.05$). (Scale bar, 50 μm.)

Role of Mechanical Strains and Cell-Shape Change During Gastrulation of *N. vectensis*. To monitor the morphogenetic movements and the dynamics of cell-shape changes during gastrulation, we generated a transgenic line expressing the actin-binding protein lifeact-mOrange2 under the control of a recently reported EF1a promoter (54). During gastrulation, presumptive endodermal cells constrict apically, forming a preendodermal plate, which then invaginates into the blastocoel (Movie S1) (40, 41). At the same time, ectodermal cells surrounding the blastopore also undergo extensive morphogenetic changes. The analysis of the time-lapse movies of gastrulating embryos of *Nematostella* revealed that the formation and invagination of the preendodermal plate correlates with extensive elongation of the ectodermal blastopore lip cells, whereas the shape of more aboral cells remains unchanged (Fig. 4*A*, Fig. S4 *A–I*, and Movies S1 and S2). Shortly after, the blastoporal cells constrict on the basal side, thus bending the blastopore lip toward the preendodermal plate and therefore pushing it inside (Fig. 4*D*). Unexpectedly, ML-7 treatment only slightly inhibits apical constriction of the preendodermal cells, and blastoporal cells abutting the preendodermal plate get stretched apically as in the control embryo (Fig. 4 *A–C*). However, sagittal sections of the ML-7–treated gastrulae revealed that the blastoporal marginal cells do not constrict on the basal side (Fig. 4*C*), and hence the blastopore lip does not bend inwards. As a result, the blastopore lip is unable to push in the preendodermal plate during gastrulation. These results suggest that cellular contractility at the basal side of the blastopore lip cells is very important for the morphogenetic movements during gastrulation. We propose that the pushing force of the blastopore lip rather than a pulling force of the apical constriction of the preendodermal cells is a driving force of invagination movement.

Regardless, the fact that blocking actomyosin contraction during gastrulation abolishes expression of several β-catenin target genes (47, 53), such as *brachyury*, *foxA*, *axin*, and *apc*, expressed in the blastopore lip (Fig. S3). Interestingly, ML-7 treatment did not affect *snailA* expressin in the preendodermal plate (Fig. S3 *K* and *L*). These results suggest that the blastopore lip is a sensitive region for β-catenin–dependent mechanotransduction.

To get insights into the mechanical properties of the cells during gastrulation, we used a Brillouin scattering microscope,

DEVELOPMENTAL BIOLOGY

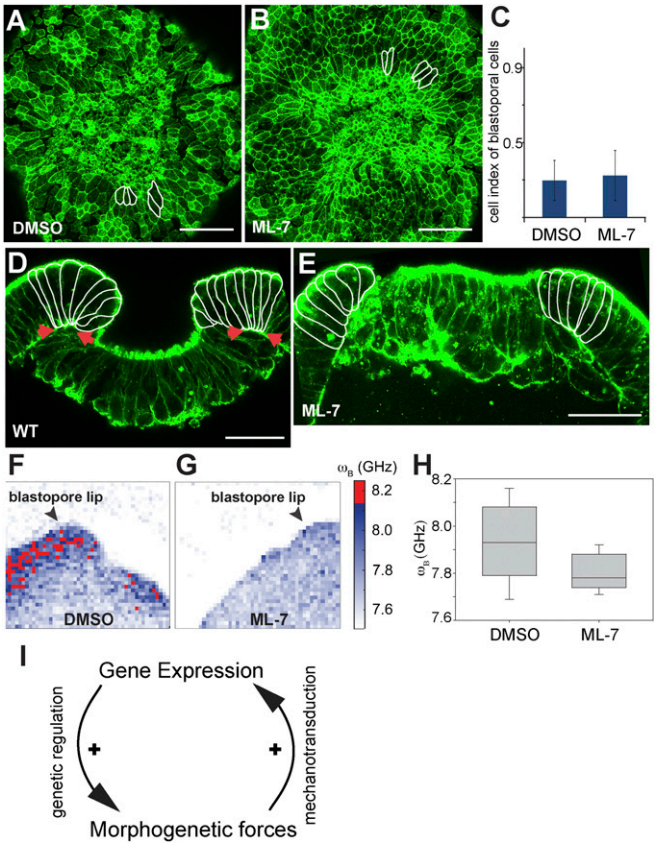

Fig. 4. Effects of ML-7 treatment on blastopore lip cell morphology and stiffness. (*A* and *B*) Oral view of the preendodermal plate and surrounding blastopore lip without (*A*) and with ML-7 (*B*) treatment, phalloidin staining. A few blastopore lip cells are outlined to emphasize the cell shape. (*C*) Differences between cell indexes of blastopore lip cells under DMSO and ML-7 treatment is not significant, paired two-tailed Student's *t* test ($P > 0.1$). (*D* and *E*) Sagittal view of the preendodermal plate and blastopore lip without (*D*) and with ML-7 (*E*) treatment. Blastopore lip cells are outlined. Arrows indicate the basal constriction of the blastopore lip cells in a control embryo, phalloidin staining. (Scale bar, 50 μm.) (*F* and *G*) Representative maps of the Brillouin frequency shift ω_B (proportional to the square root of the longitudinal storage modulus) in the vicinity of the blastopore lip without (*F*) and with (*G*) inhibitor treatment, showing a decrease in stiffness in the treated samples. Regions of high-frequency shift (stiffness) are colored red. Arrowheads mark the blastopore lip region. (*H*) Frequency shift ω_B (which is proportional to the square root of the elastic modulus) in embryos with and without inhibitor. The untreated embryos show an increased frequency shift on average and broader distribution of values relative to the treated ones. (*I*) Proposed positive feedback model of regulating gene expression and cell-shape changes with inherent mechanical stress.

which allows for spatial mapping of the viscoelastic properties of biological materials (55–58). The Brillouin microscope probes the sample pixel per pixel with a single-frequency laser and measures the gigahertz scale (<0.0001-nm wavelength) spectral modification of the scattered light. Spectrally shifted light is the result of inherent collective thermal density fluctuations within the sample, which can be used to calculate the viscoelasticity of the cell.

Our measurements show that the blastopore lip cells appear significantly "stiffer" than the plate cells or cells on the aboral side of the embryo (the elastic modulus in the former is larger than in the latter by on average more than 10%) (Fig. S4 *J* and *K*). Remarkably, cells of the ML-7–treated embryos were significantly softer than cells of the wild-type embryos and blastopore lip cells displayed a similar stiffness as the other parts of the embryo (Fig. 4 *E*–*I*). Our data suggest that contractility and increased longitudinal compressibility (stiffness) of the blastopore lip cells is crucial for the force generation, which drives invagination movements and facilitates mechanosensitive gene expression.

Discussion

Our results show that in *Nematostella*, *brachyury* expression can be induced by β-catenin–dependent mechanotransduction of physical forces. We speculate that during normal development, the gastrulation movements generate the physical forces acting on blastopore lip cells. We propose that mechanical and genetic regulation of gene expression form a feedback loop that robustly enforces *brachyury* expression: early maternal activation of intracellular components of Wnt/β-catenin at the oral pole activate the expression of Wnt ligands in the preendodermal plate at the blastula stage (Fig. 4*I*). Through negative feedback loops, these Wnt genes become expressed as a ring surrounding the preendodermal plate, where they initiate *brachyury* expression at the margin of the blastopore and endoderm in the plate. The contractility of the blastopore lip cells lead to a local higher stiffness. This mechanical stress is then transduced in a β-catenin–dependent manner to enforce *brachyury* expression and other targets of β-catenin in the blastopore lip. Due to the high concentrations of β-catenin at the oral pole, this region is particularly competent to respond to mechanical stress, preventing that undirected physical forces could ectopically activate *brachyury* expression. However, upon prolonged physical stress, *brachyury* can be induced ectopically as well. The contraction of the blastopore lip cells at the basal side then bends the lip inward and pushes the plate into the blastocoel.

Because β-catenin–dependent mechanotransduction and activation of *brachyury* is also found in other Bilateria (16), these findings imply that this mechanism of gene regulation and the feedback between genetic and mechanical gene activation might be an ancient feature of animal development, at least predating the cnidarian–bilaterian split over 600 Mya (23, 24).

Materials and Methods

Animals and Embryo Culturing. Animals were kept in the dark at 18 °C. Spawning and embryo collection were performed as described (59, 60). Work with genetically modified organisms (GMO) of safety level 1 at the Department of Molecular Evolution and Development, University of Vienna, was approved by the Ministery of Economy and Sciences (BMWfW) of Austria.

Live Imaging. Transgenic animals expressing lifeact-mOrange2 under control of the ubiquitous EF1α promoter were generated. Fully transgenic F1 animals were spawned as described (59, 60). Transgenic embryos were embedded in 1% low-melting point agarose (V3841, Promega) and imaged in *Nematostella* medium (NM) with a HCX ApoL40X/0.8W objective using a Leica TCS SP5X confocal microscope. Time stamps were added to the movies using ImageJ software Time Stamper plugin (NIH).

Morpholino Injection. β-Catenin knockdown was performed by zygote injection of previously characterized translation blocking β-cat–MO: 5′ TTCTTCGACTTTAAATCCAACTTCA (53) at a concentration of 500 μM.

Inhibitor Treatment. Prior treatment embryos were kept at 17 °C. For the inhibition of cellular contractility and cellular mechanical tensions within the embryo, ML-7, a selective MLCK inhibitor, was used (Calbiochem, Merk Millipore). All treatments were carried out at 22 °C. At 16 hpf, precisely staged spherical blastulae were selected and treated with 10 μM ML-7/1% DMSO in NM until 28 hpf. Control embryos were treated with 1% DMSO in NM. At least 100 embryos were selected for each treatment, including the experiments with embryo compression. At 28 hpf, embryos were processed for the fixation as described below. To confirm reversibility of ML-7 treatment, at 28 hpf, ML-7–treated embryos were washed 5 × 5 min in NM and left to develop in NM until 42 hpf.

Uniaxial Global Embryo Compression. To restore mechanical strains in ML-7–inhibited embryos, we applied uniaxial global embryo compression to the embryos. For this purpose, we placed exactly 100 embryos on a Petri plate lined with 1.1% low-melting point agarose/10 μM ML-7/NM) in the 10 μM ML-7/1% DMSO/NM solution. Microscopic coverslip size 24 × 50 mm, m = 0.43 g

(Roth, catalog no. 1871) was slowly dragged on top of the embryos without further pressing. In this way, the force compressing the embryos was approximately equivalent to the weight of the coverslip. Since the number of embryos in each experiment was 100, the compressing force was roughly the same in each experiment, which was calculated as: $F = m_{coverslip} \cdot g - Fa$; $Fa = \rho_{water} \cdot g \cdot V_{coverslip}$; $F = 2.61$ mN on 100 embryos. Therefore, ~26 μN was applied to each embryo. Embryos were compressed for 12 h at 22 °C. Three independent experiments were performed. To stimulate ectopic *brachyury* expression, we compressed stage-matched spherical blastulae at 16 hpf and late gastrulae at 28 hpf for 26 h at 16 °C.

Phalloidin Staining. Embryos were fixed in 3.7% formaldehyde/PBS at 4 °C for 1 h. After 7 min acetone shock on ice, embryos were washed five times in PBSTx (PBS with 0.2% Triton X-100) and incubated with Alexa Fluor 488 Phalloidin (Thermo Fisher Scientific) diluted 1:30 in PBSTx at 4 °C, overnight. After the staining, embryos were washed 10 × 10 min in PBSTx, mounted in Vectashield (Vector Laboratories), and imaged with a Leica TCS SP5X confocal microscope.

In Situ Hybridization. In situ hybridizations (ISHs) were conducted as previously described (48, 61). Embryos were imaged and quantified with the Nikon Eclipse 80i compound microscope equipped with DIC optics and Zeiss AxioCam camera. Quantification of the in situ patterns of different treatments within one experiment was done blindly on encoded microscope slides.

Brillouin Scattering Microscopy.

Experimental setup. The setup used for Brillouin scattering microscopy employs a confocal microscope with a high-efficiency cross-dispersion imaging spectrometer described in detail in ref. 58. The only significant difference was the addition of a Lyot stop to suppress high-frequency interference fringes (57) before the spectrum being imaged onto an EM CCD camera. Embryos were embedded in low-melting point agarose as described above and imaged through glass-bottom dishes in a custom sample holder mounted on a 3-axis Piezo stage, which was mounted on a motor stage, and spatial maps of the frequency shift were obtained by translating the sample. In all cases we measured the parallel polarization back-scattering spectra. A transmitted light image could be obtained by illuminating the sample from above via a condenser to image onto a sCMOS camera attached to a side port of the microscope frame.

Imaging. A 1.4 N.A. oil-immersion objective lens (Olympus PLAPON 60XOSC2) was used for excitation/detection. An iris positioned at the entrance port of the microscope was partially closed to reduce the effective N.A. and peak broadening (62). Measurements on 100 nm fluorescent beads yielded a point spread function with a full width at half maximum of 340 nm (690 nm) laterally (axially). In all scans, the laser power at the sample was between 1 and 3 mW and acquisition time per spectrum was between 100 and 300 ms. Depending on the size, a Brillouin map would typically take several to tens of minutes. Wide-field images were taken before and after scans to assure embryos had not moved or changed significantly during the scan.

Data analysis. Calibration measurements were performed between sample measurements on water and ethanol to calibrate the dispersion axis as described in ref. 58. Least-squares fitting of Voigt functions in Matlab (Matlab peakfit.m function: https://terpconnect.umd.edu/~toh/spectrum/InteractivePeakFitter.htm) was used to determine the separation of the peaks along the dispersion axis, which together with the calibration measurements allowed us to deduce the Brillouin frequency shift (ω_B) (56, 58).

Data interpretation. All spatial maps show the Brillouin frequency shift (derived from the mean position of the fitted peaks in the measured spectrum). The frequency shift is related to the longitudinal storage modulus (M') via: $\omega_B = C \cdot n \cdot \lambda^{-1} \sqrt{M'/\rho}$, where n and ρ are the refractive index and mass density of the sample at the measured point, λ is the wavelength of the laser used, and C is a constant that depends on the measurement geometry. It is often observed and can be argued via Lorenz–Lorentz relation that the refractive index squared will scale with the mass density, such that variations in these parameters in a heterogeneous sample will to a good approximation cancel each other out. From this it follows that the longitudinal storage modulus will be proportional to the square of the measured Brillouin frequency shift.

Interpretation of the measured longitudinal storage modulus (M′). M′ is distinct from the Young's Modulus E [as is measured e.g., with atomic force microscopy (AFM)] in that it assumes that laterally the sample size is constrained. It thereby is sensitive to the compressibility of the sample and can be related to E only with knowledge of the Poisson ratio. A large value of M′ would thus mean that if the sample's lateral dimensions are fixed, its longitudinal dimensions (in the direction the sample is probed) would change less when subject to a stress (i.e., it is more "rigid"). It is also worth noting that in Brillouin light scattering, one is measuring the elastic modulus at gigahertz frequencies, compared with the quasistatic regime probed using most perturbation-based techniques. At these frequencies, most materials are at or above their glass transition frequency and thus will appear significantly stiffer. Nevertheless in live cells, an empirical power–law relation between the AFM-measured Young's modulus and the Brillouin-measured longitudinal modulus is often observed (56), suggesting that an increase in the measured Brillouin frequency shift may be assumed to be associated with an increase in the stiffness of cells.

Image Processing. Images were adjusted for levels, brightness, and contrast using FIJI software (63). Focus stacking of ISH images was done using Helicon Focus software (Helicon Soft Ltd). All images were cropped and assembled into the panels using Adobe Illustrator CS6 software.

Cell-Shape Index Measurement. Cell-shape indexes of the blastoporal and aboral cells for the beginning of gastrulation (t0) and for the midgastrulation time point (t1) were calculated as follows: cell index(t) = cell width(t)/cell length(t). Fold change cell index was calculated as cell index(t0)/cell index (t1). $n = 30$, $P \leq 0.01$, paired two-tailed Student's t test. Nondividing cells visible in the middle of the field of view were taken at random for measurements.

ACKNOWLEDGMENTS. We thank Carl-Philipp Heisenberg and Cornelia Schwayer for fruitful discussions, G. Genikhovich for critically reading the first version of the manuscript, E. L. Genikhovich for help in calculating the applied force, and the Advanced Microscopy Facility in Vienna Biocenter Facilities and the Core Facility for Cell Imaging and Ultrastructure Research of the University of Vienna for assistance. This work was funded by Austrian Science Fund Grant P25993 (to U.T.).

1. Wozniak MA, Chen CS (2009) Mechanotransduction in development: A growing role for contractility. *Nat Rev Mol Cell Biol* 10:34–43.
2. Iskratsch T, Wolfenson H, Sheetz MP (2014) Appreciating force and shape—The rise of mechanotransduction in cell biology. *Nat Rev Mol Cell Biol* 15:825–833.
3. Lecuit T, Lenne P-F, Munro E (2011) Force generation, transmission, and integration during cell and tissue morphogenesis. *Annu Rev Cell Dev Biol* 27:157–184.
4. Hoffman BD, Grashoff C, Schwartz MA (2011) Dynamic molecular processes mediate cellular mechanotransduction. *Nature* 475:316–323.
5. Wang N, Tytell JD, Ingber DE (2009) Mechanotransduction at a distance: Mechanically coupling the extracellular matrix with the nucleus. *Nat Rev Mol Cell Biol* 10:75–82.
6. Chen CS (2008) Mechanotransduction–A field pulling together? *J Cell Sci* 121: 3285–3292.
7. Gillespie PG, Walker RG (2001) Molecular basis of mechanosensory transduction. *Nature* 413:194–202.
8. Wang N, Butler JP, Ingber DE (1993) Mechanotransduction across the cell surface and through the cytoskeleton. *Science* 260:1124–1127.
9. Vogel V, Sheetz M (2006) Local force and geometry sensing regulate cell functions. *Nat Rev Mol Cell Biol* 7:265–275.
10. Folkman J, Moscona A (1978) Role of cell shape in growth control. *Nature* 273:345–349.
11. Chen CS, Mrksich M, Huang S, Whitesides GM, Ingber DE (1997) Geometric control of cell life and death. *Science* 276:1425–1428.
12. McBeath R, Pirone DM, Nelson CM, Bhadriraju K, Chen CS (2004) Cell shape, cytoskeletal tension, and RhoA regulate stem cell lineage commitment. *Dev Cell* 6: 483–495.
13. Engler AJ, Sen S, Sweeney HL, Discher DE (2006) Matrix elasticity directs stem cell lineage specification. *Cell* 126:677–689.
14. Nelson CM, et al. (2005) Emergent patterns of growth controlled by multicellular form and mechanics. *Proc Natl Acad Sci USA* 102:11594–11599.
15. Mammoto T, et al. (2011) Mechanochemical control of mesenchymal condensation and embryonic tooth organ formation. *Dev Cell* 21:758–769.
16. Brunet T, et al. (2013) Evolutionary conservation of early mesoderm specification by mechanotransduction in Bilateria. *Nat Commun* 4:2821.
17. Kornikova ES, Korvin-Pavlovskaya EG, Beloussov LV (2009) Relocations of cell convergence sites and formation of pharyngula-like shapes in mechanically relaxed Xenopus embryos. *Dev Genes Evol* 219:1–10.
18. Kornikova ES, Troshina TG, Kremnyov SV, Beloussov LV (2010) Neuro-mesodermal patterns in artificially deformed embryonic explants: A role for mechano-geometry in tissue differentiation. *Dev Dyn* 239:885–896.
19. Beloussov LV, Luchinskaya NN, Ermakov AS, Glagoleva NS (2006) Gastrulation in amphibian embryos, regarded as a succession of biomechanical feedback events. *Int J Dev Biol* 50:113–122.
20. Farge E (2003) Mechanical induction of Twist in the Drosophila foregut/stomodeal primordium. *Curr Biol* 13:1365–1377.
21. Hove JR, et al. (2003) Intracardiac fluid forces are an essential epigenetic factor for embryonic cardiogenesis. *Nature* 421:172–177.
22. Hiramatsu R, et al. (2013) External mechanical cues trigger the establishment of the anterior-posterior axis in early mouse embryos. *Dev Cell* 27:131–144.

23. Park E, et al. (2012) Estimation of divergence times in cnidarian evolution based on mitochondrial protein-coding genes and the fossil record. *Mol Phylogenet Evol* 62: 329–345.
24. Reis dos M, et al. (2015) Uncertainty in the timing of origin of animals and the limits of precision in molecular timescales. *Curr Biol* 25:2939–2950.
25. Technau U (2001) Brachyury, the blastopore and the evolution of the mesoderm. *BioEssays* 23:788–794.
26. Arendt D, Technau U, Wittbrodt J (2001) Evolution of the bilaterian larval foregut. *Nature* 409:81–85.
27. Technau U, Bode HR (1999) HyBra1, a Brachyury homologue, acts during head formation in Hydra. *Development* 126:999–1010.
28. Kispert A, Herrmann BG, Leptin M, Reuter R (1994) Homologs of the mouse Brachyury gene are involved in the specification of posterior terminal structures in Drosophila, Tribolium, and Locusta. *Genes Dev* 8:2137–2150.
29. Spring J, et al. (2002) Conservation of brachyury, Mef2, and snail in the myogenic lineage of jellyfish: A connection to the mesoderm of bilateria. *Dev Biol* 244:372–384.
30. Marcellini S, Technau U, Smith JC, Lemaire P (2003) Evolution of brachyury proteins: Identification of a novel regulatory domain conserved within bilateria. *Dev Biol* 260: 352–361.
31. Lartillot N, Lespinet O, Vervoort M, Adoutte A (2002) Expression pattern of brachyury in the mollusc patella vulgata suggests a conserved role in the establishment of the AP axis in bilateria. *Development* 129:1411–1421.
32. Gross JM, McClay DR (2001) The role of brachyury (T) during gastrulation movements in the sea urchin Lytechinus variegatus. *Dev Biol* 239:132–147.
33. Yamada A, Pang K, Martindale MQ, Tochinai S (2007) Surprisingly complex T-box gene complement in diploblastic metazoans. *Evol Dev* 9:220–230.
34. Technau U, Miller MA, Bridge D, Steele RE (2003) Arrested apoptosis of nurse cells during Hydra oogenesis and embryogenesis. *Dev Biol* 260:191–206.
35. Smith JC, Price BMJ, Green JBA, Weigel D, Herrmann BG (1991) Expression of a Xenopus homolog of brachyury (T) is an immediate-early response to mesoderm induction. *Cell* 67:79–87.
36. Arnold SJ, et al. (2000) Brachyury is a target gene of the Wnt/β-catenin signaling pathway. *Mech Dev* 91:249–258.
37. Turner DA, Rué P, Mackenzie JP, Davies E, Martinez Arias A (2014) Brachyury cooperates with Wnt/β-catenin signalling to elicit primitive-streak-like behaviour in differentiating mouse embryonic stem cells. *BMC Biol* 12:63.
38. Yamaguchi H, Kitagawa Y, Miki K (1999) Brachyury regulatory region active in embryonal carcinoma P19 cells. *Biosci Biotechnol Biochem* 63:608–609.
39. Vonica A, Gumbiner BM (2002) Zygotic Wnt activity is required for brachyury expression in the early Xenopus laevis embryo. *Dev Biol* 250:112–127.
40. Kraus Y, Technau U (2006) Gastrulation in the sea anemone Nematostella vectensis occurs by invagination and immigration: An ultrastructural study. *Dev Genes Evol* 216: 119–132.
41. Magie CR, Daly M, Martindale MQ (2007) Gastrulation in the cnidarian Nematostella vectensis occurs via invagination not ingression. *Dev Biol* 305:483–497.
42. Saitoh M, Ishikawa T, Matsushima S, Naka M, Hidaka H (1987) Selective inhibition of catalytic activity of smooth muscle myosin light chain kinase. *J Biol Chem* 262: 7796–7801.
43. Bain J, McLauchlan H, Elliott M, Cohen P (2003) The specificities of protein kinase inhibitors: An update. *Biochem J* 371:199–204.
44. Lee J-Y, Harland RM (2010) Endocytosis is required for efficient apical constriction during Xenopus gastrulation. *Curr Biol* 20:253–258.
45. Wikramanayake AH, et al. (2003) An ancient role for nuclear beta-catenin in the evolution of axial polarity and germ layer segregation. *Nature* 426:446–450.
46. Scholz CB, Technau U (2003) The ancestral role of brachyury: Expression of NemBra1 in the basal cnidarian Nematostella vectensis (Anthozoa). *Dev Genes Evol* 212:563–570.
47. Röttinger E, Dahlin P, Martindale MQ (2012) A framework for the establishment of a cnidarian gene regulatory network for "endomesoderm" specification: The inputs of ß-catenin/TCF signaling. *PLoS Genet* 8:e1003164.
48. Kraus Y, Aman A, Technau U, Genikhovich G (2016) Pre-bilaterian origin of the blastoporal axial organizer. *Nat Commun* 7:11694.
49. Ikmi A, McKinney SA, Delventhal KM, Gibson MC (2014) TALEN and CRISPR/Cas9-mediated genome editing in the early-branching metazoan Nematostella vectensis. *Nat Commun* 5:5486–5488.
50. Hwang WY, et al. (2013) Efficient genome editing in zebrafish using a CRISPR-Cas system. *Nat Biotechnol* 31:227–229.
51. Wiedenheft B, Sternberg SH, Doudna JA (2012) RNA-guided genetic silencing systems in bacteria and archaea. *Nature* 482:331–338.
52. Stamos JL, Weis WI (2013) The β-catenin destruction complex. *Cold Spring Harb Perspect Biol* 5:a007898.
53. Leclère L, Bause M, Sinigaglia C, Steger J, Rentzsch F (2016) Development of the aboral domain in Nematostella requires β-catenin and the opposing activities of Six3/6 and Frizzled5/8. *Development* 143:1766–1777.
54. Steinmetz PRH, Aman A, Kraus JEM, Technau U (2017) Gut-like ectodermal tissue in a sea anemone challenges germ layer homology. *Nat Ecol Evol* 1:1535–1542.
55. Antonacci G, Braakman S (2016) Biomechanics of subcellular structures by non-invasive Brillouin microscopy. *Sci Rep* 6:37217.
56. Scarcelli G, et al. (2015) Noncontact three-dimensional mapping of intracellular hydromechanical properties by Brillouin microscopy. *Nat Methods* 12:1132–1134.
57. Edrei E, Gather MC, Scarcelli G (2017) Integration of spectral coronagraphy within VIPA-based spectrometers for high extinction Brillouin imaging. *Opt Express* 25: 6895–6903.
58. Elsayad K, et al. (2016) Mapping the subcellular mechanical properties of live cells in tissues with fluorescence emission-Brillouin imaging. *Sci Signal* 9:rs5.
59. Genikhovich G, Technau U (2009) Induction of spawning in the starlet sea anemone Nematostella vectensis, in vitro fertilization of gametes, and dejellying of zygotes. *Cold Spring Harb Protoc* 2009:pdb.prot5281.
60. Fritzenwanker JH, Technau U (2002) Induction of gametogenesis in the basal cnidarian Nematostella vectensis(Anthozoa). *Dev Genes Evol* 212:99–103.
61. Genikhovich G, Technau U (2009) In situ hybridization of starlet sea anemone (Nematostella vectensis) embryos, larvae, and polyps. *Cold Spring Harb Protoc* 2009: pdb.prot5282.
62. Antonacci G, Foreman MR, Paterson C, Toeroek P (2013) Spectral broadening in Brillouin imaging. *Appl Phys Lett* 103:221105.
63. Schindelin J, et al. (2012) Fiji: An open-source platform for biological-image analysis. *Nat Methods* 9:676–682.